2014 IEEE International Conference on Robotics & Automation (ICRA)
Hong Kong Convention and Exhibition Center
May 31 - June 7, 2014. Hong Kong, China

Internal Impedance Control helps Information Gain in Embodied Perception

Nantachai Sornkarn[1], Matthew Howard[1] and Thrishantha Nanayakkara[1]

***Abstract*— Internal impedance is one of the key factors determining the quality of embodied perception and action in biological organisms and robots. Though the role of impedance control in robotic actuation has been well studied, its significance in the accuracy of proprioception with embodied sensors is not well known yet. Therefore, it is important to characterize the relationship between the entropy of sensor information and the impedance of their physical embodiment, through which sensors feel the internal state of the body and the environment. In this paper, we address the role of internal impedance in the accuracy of embodied perception. To investigate this, we pose the problem of using only torque data measured at the stationary base of a two link planar manipulator, to estimate the deflection caused by an external torque in the McKibben type pivot joint with variable stiffness. Based on analytical modelling and experimental validation, this paper presents, for the first time, that non-linear static memory primitives relating internal impedance, internal kinematic variables, and forces felt at the base of the manipulator - similar to the functionality of tendon organs of biological counterparts - can be used to tune optimal internal impedance parameters to maximize the accuracy of internal state estimation during external perturbations.**

I. Introduction

Embodied sensing in a biological system such as mechanoreceptors in the hand [1], are modulated by the physical changes of the body [2]. This in-turn influences the sensorimotor coupling network resulting in changes in behavior [3]. For instance, as we are required to estimate the weight of an object, we would not hold it with a stiff hand. Instead, we bring the internal impedance of the hand to some optimal state and gently bob the object up and down to use proprioceptive feedback to estimate its weight. This can be skilfully utilized to maximize information gain in sensing to control underactuated robots. As signified in recent findings in passive compliance of biological musculoskeletal systems [4], control of dynamic interactions with the environment can be simplified through its embodiment itself. Therefore, recent findings in the emergence of adaptive behaviors of muscular-hydrostats like octopus due to its ability to control the stiffness distribution and morphology of the body [5], has caught a lot of attention among the robotics research community [6], [7].

An essential set of mathematical tools to understand the role of internal impedance in control of dynamic systems were first laid down by Hogan in [8]. Hogan's theory proposes that a body in dynamic contact with the environment should be able to adapt its internal impedance (stiffness, damping, and inertia parameters) in order to maintain a stable dynamic coupling with the environment. However, the main focus of the robotics community has so far been on internal impedance control for effective actuation than its role in perception, especially in proprioception. For instance, impedance control in the joint space has been achieved for rigid body robotic digging [9], direct contact with humans in robotic massage systems [10], companions for humans [**?**], human motor rehabilitation [11], adaptive prosthetic limbs [12], adaptive exoskeletons [13].

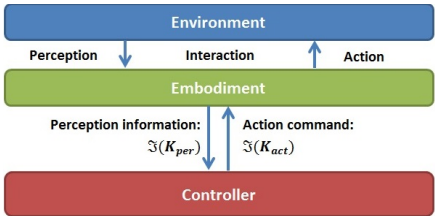

Fig. 1. In an embodied system, the system interacts with the environment through its embodied structure. The internal impedance required for accurate perception through its embodied sensor can differ from that required to take appropriate action. Taken action with an appropriate impedance could likewise effect the quality of perception of the environment.

Robotic active perception has also attracted recent attention especially in the context of vision [14]. Though active exploration for visual cues in the external world has been widely studied for instance in recognition and exploration of robot's activities while interacting with environment [15], active exploration in the internal impedance domain for enhanced proprioception has not been studied so far.

Passive dynamics based locomotion is another interesting area of research that views embodiment as a powerful infrastructure to emerge behavior with no sensing at all. Passive dynamic walkers presented in [16] use solely the interaction between the walker and the environment to emerge a metastable walking behavior. In fact, it seems that biological evolution too solve the problem of energy efficient locomotion through tuning the embodiment to be able to harness energy from the environment as shown in an experiment where a dead trout swimming against a water stream [17]. As opposed to a fully actuated robotic fish [18]; an underactuated robotic fish that utilizes the passive dynamics of the embodiment with single actuator and multiple passive variable stiffness joint, is proven to be more energy efficient while being able to emerge more

The work described in this paper is supported by STIFFFLOP project grant from the European Communities Seventh Framework Programme under grant agreement 287728. www.stiff-flop.eu

[1]Nantachai Sornkarn, Matthew Howard, and Thrishantha Nanayakkara are with Centre For Robotics Research, Department of Informatics, King's College London, WC2R 2LS London, UK nantachai.sornkarn@kcl.ac.uk

natural movements [19].

In general, the implications of the embodiment concept are mostly studied in the context of enhancing the actuation, visual perception, or as an assistive element in granting, or enhancing stability in locomotion. They take advantage of passive body dynamics and the interaction with environment to achieve the required goals without a rather high-level cognitive processes [20].

From embodied perception perspective, a major challenge in this study is to investigate how body's internal impedance can be regulated to gain the accurate perception. This paper focuses on the role of internal impedance modulation in the embodied perception of a simple planar 2-links manipulator system with variable joint stiffness. The experimental results are used to approximate the stiffness calibration curve for different pre-tension states of the stiffness element. We use the transfer entropy from Kullback Leibler divergence approach as an indicator to the information gain across pre-tension state of the stiffness element. Newton-Raphson optimization and Hooke-Jeeves pattern search are compared to search for the best pre-tension state that maximizes transfer entropy to arrive at a best estimate for angular displacement of a joint between two links given the torque measured at the base.

This paper is structured as follows. First the experimental platform is described, including the joint stiffness model's numerical simulation, followed by the methodology employed in the experiments. Thereafter, results and analysis are exhibited. Lastly, the paper is discussed and concluded.

II. Experimental Setup

A. Manipulator Platform with Variable Joint Stiffness

A design of the antagonistic manipulator used in the experiment consists of two manipulator links - base link of length $l_1 = 15$ cm, and an upper link of length $l_2 = 17$ cm. The design of the variable joint stiffness in this platform is based on the 'Mechanically Controlled Stiffness' approach [21].The stiffness of the McKibben type pivot joint between these two links can be adjusted by moving the anchor point of the two springs as shown in figure 2 and figure 3. As depicted in figure 3, the angle α between each lever arm and the centre of link 2 can be pre-configured; and the springs can be preloaded by changing the position of the anchor point. The system is mounted on a table and fixed with a clamp underneath. Apart from ball bearings, the whole system is designed in SolidWorks and fabricated from ABS plastic using the Dimension SST768 3D-printer. In this experiment, we focus mainly on the perception of the angular displacement θ_2 of the upper link relative to the base link based on the torque τ_f sensed at the base of the manipulator around z-axis using a ATI Mini40 six axis force/torque (F/T) transducer at 100 Hz. For verification of the accuracy of estimating θ_2, we used an XSENS MTx wireless motion capturing sensor sampled at 100 Hz as shown in figure 2.

B. Joint Stiffness Model

From figure 3, the distance between the axis of the pivot joint and the anchor point of the two springs at rest is denoted by l_d. The resting lengths of each spring are r_1 and r_2. The length of the lever arms connected at the two free ends of the springs are $d = 3$ cm. The changes in the length of each spring are denoted by Δr_1 and Δr_2.

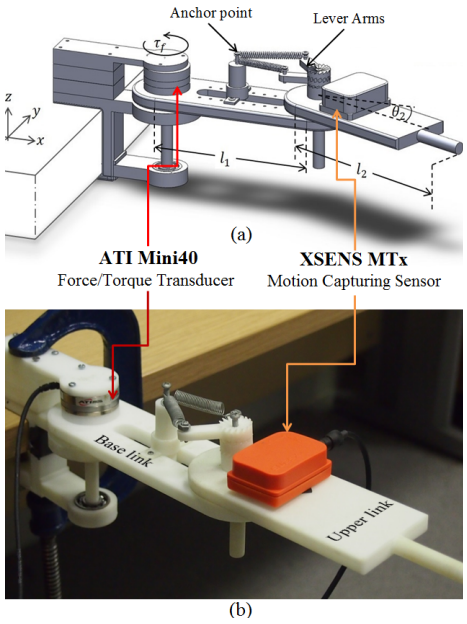

Fig. 2. (a) a design of two-links planar manipulator with a variable stiffness joint. The rotational displacement of the upper link, θ_2, is recorded using an XSENS MTx Motion Capturing sensor; whereas the torque experienced at the base of the manipulator during such movement is measured by ATI Mini40 6-axis Force/Torque Transducer, (b) a photo of the experimental platform attached on the table with a clamp.

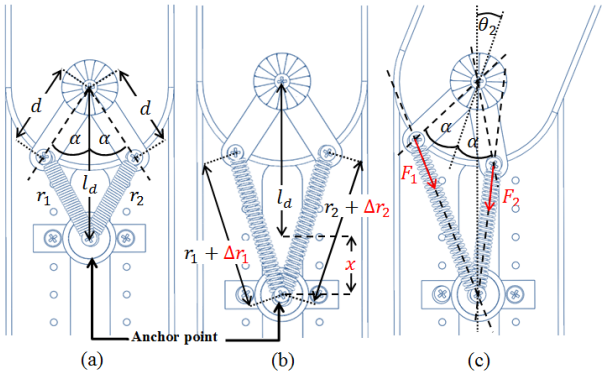

Fig. 3. Top view of the manipulator, focusing on the variable stiffness element at the joint. (a) Joint stiffness configuration, when $\theta_2 = 0$ and the stiffness elements are mounted at the origin point. (b) Joint stiffness configuration, when $\theta_2 = 0$ and both springs are extended by moving the anchor point. (c) Second joint is rotated at particular angle θ_2

From figure 3 (a), the resting lengths of both springs can be computed as given by

$$r_i = \sqrt{{l_d}^2 + d^2 - 2dl_d \cos \alpha_i}. \quad (1)$$

where $i = 1, 2$.

Hence, from figure 3 (b) and (c) we can obtain the resulting length of both springs due to the change of both

joint angular position, θ_2, and the position of the anchor point, x, as following.

$$r_1 + \Delta r_1 = \sqrt{(l_d + x)^2 + d^2 - 2d(l_d + x)\cos(\alpha + \theta_2)}$$
$$r_2 + \Delta r_2 = \sqrt{(l_d + x)^2 + d^2 - 2d(l_d + x)\cos(\alpha - \theta_2)} \quad (2)$$

Given that each spring constant K_i of the stiffness elements are known, the force contribution $\vec{F}_{si}$ by each spring at the pivot can be calculated based on the kinematic relations shown in figure 3 (c) as given by

$$\vec{F}_{si} = \Delta r_i K_i \quad (3)$$

Hence, the torques around the pivot axis developed by both stiffness elements can be found by

$$\tau_i = \vec{F}_{si} \times l_d + x = \vec{F}_{si\perp}(l_d + x), \quad (4)$$

where $\vec{F}_{si\perp}$ is the force acting perpendicular to the base link at the pivot joint given by

$$\frac{d\sin(\alpha + \theta_2)}{r_1 + \Delta r_1} = \frac{\vec{F}_{s1\perp}}{\vec{F}_{s1}} \quad \rightarrow \quad \vec{F}_{s1\perp} = \vec{F}_{s1}\frac{d\sin(\alpha + \theta_2)}{r_i + \Delta r_1} \quad (5)$$
$$\frac{d\sin(\alpha - \theta_2)}{r_2 + \Delta r_2} = \frac{\vec{F}_{s2\perp}}{\vec{F}_{s2}} \quad \rightarrow \quad \vec{F}_{s2\perp} = \vec{F}_{s2}\frac{d\sin(\alpha - \theta_2)}{r_i + \Delta r_2} \quad (6)$$

From equations (4), (5), and (6), the stiffness-element-contributed torque perceived at the base link can then be computed as given by

$$\tau_{s1} = \vec{F}_{s1}\frac{d\sin(\alpha + \theta_2)}{r_1 + \Delta r_1}(l_d + x), \quad (7)$$
$$\tau_{s2} = \vec{F}_{s2}\frac{d\sin(\alpha - \theta_2)}{r_2 + \Delta r_2}(l_d + x), \quad (8)$$
$$\tau_s = \tau_{s1} + \tau_{s2}. \quad (9)$$

Then we simulated the torque perceived at the base by changing the pre-tension state of x between $4, \cdots, 8$ cm for $\alpha_i = 55^\circ$ and 25° in order to ascertain the landscape of the torque felt at the base τ_f as a function of relative angular displacement θ_2 of the upper link and the pre-tension state x of the stiffness element. From figure 4 we can note that the level of non-linearity in this landscape tends to decrease to almost a linear one when the angular configuration of the two lever arms α reduces.

Therefore, in order to study the role x of the stiffness element in the information gained by measuring the torque felt at the base τ_f to estimate θ_2, it is important to have a reasonable level of non-linearity in the above relationship shown in figure 4. In our experiments, α was set to be 55°.

III. Experiments and Results

The main purpose of our experiment is to examine the role of body internal impedance in an accurate embodied perception. In this case, we limit our study to embodied perception during slow movements, so that a static calibration of sensors can be used in a dynamic condition as static

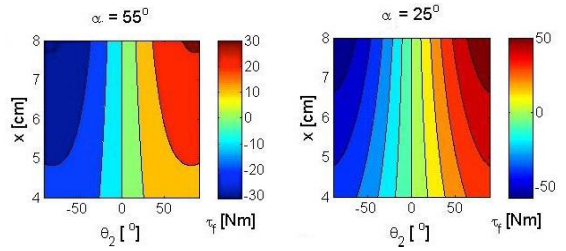

(a) (b)

Fig. 4. Contour plot of the torque perceived at the base as x varies from 4 to 8 and $\theta_2 = -90^\circ, .., 90^\circ$, when (a) $\alpha = 55^\circ$ and (b) $\alpha = 25^\circ$

memory primitives of embodiment and kinematic variables. The relative angular displacement of the upper link and the torque felt at the base in a static condition are denoted by ${\theta_2}^{sta}$ and ${\tau_f}^{sta}$ respectively, and those in a dynamic condition are denoted by ${\theta_2}^{dyn}$ and ${\tau_f}^{dyn}$ respectively. Here we investigate as to how the non-linear relationship between ${\theta_2}^{sta}$ and ${\tau_f}^{sta}$ can be exploited to search for the optimal x to maximize information gained about ${\theta_2}^{dyn}$ during a dynamic movement of the upper link (action).

A. Static Movement

As described and illustrated in section II-B, there is a non-linear characteristic presented in our design of variable joint stiffness. In order to identify the landscape of this nonlinear relationship and to construct the static memory primitives for internal state estimation, the data was recorded for 10 trials for each configuration of the stiffness element for statistic evaluation. The static torque ${\tau_f}^{sta}$ was measured at different pre-tension states, $x = 4, \cdots, 8$ cm at different ${\theta_2}^{sta}$ values. Measurements were taken after leaving the system to settle down to a steady state (ex. after the vibrations in the springs were damped out). For each trial, the recorded data is mapped using a third order best fit polynomial function. Figure 5 (a) show the variability of the fitted torque data across 10 trials for each configuration of stiffness element, $x = 4$ cm to $x = 8$ cm.

The average torque profile ${\tau_f}^{sta}$, from all 10 trials is shown in 5 (b), from which the corresponding contour representing the non-linear static memory primitives can be constructed. It should be noted that the experimental results shown in figure 5 (c) is comparable to that obtained in numerical simulation shown in figure 4 (a) (average probability of the hypothesis that the columns of figure 5 (c) are the same as those in figure 4 (a), is statistically significant in Mann-Whitney U test), confirming the validity of our analytical model.

From the relationship between the torque experienced at the base and the relative angular displacement of the upper link, the joint stiffness, $K({\theta_2}^{sta})$, can be obtained from the tangent of the function of torque with respect to the angular displacement at any given ${\theta_2}^{sta}$ as given by:

$$K({\theta_2}^{sta}) = \frac{\partial {\tau_f}^{sta}}{\partial {\theta_2}^{sta}}. \quad (10)$$

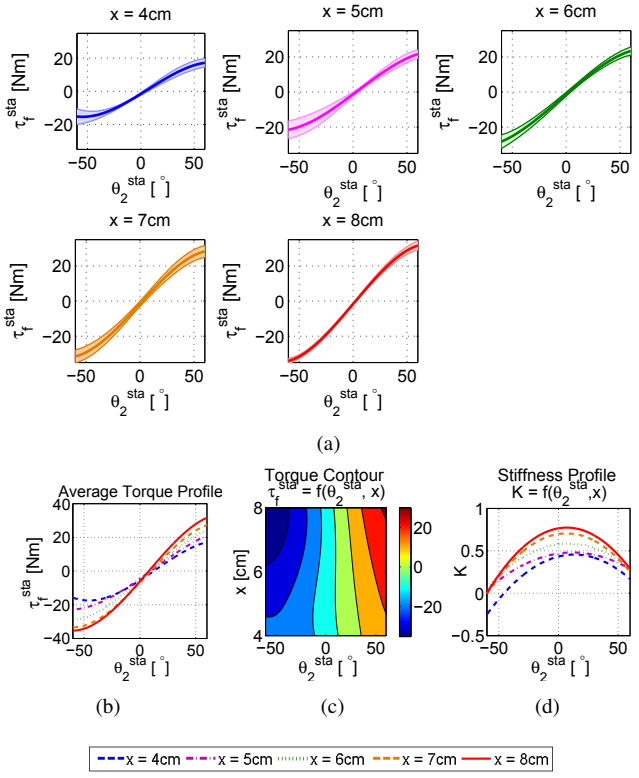

Fig. 5. (a) The variability of torque perceived at the base across 10 trials for different pre-tension states x. (b) best fit thrid order polynomials to ${\tau_f}^{sta}$ vs ${\theta_2}^{sta}$ primitives across different $x \in [4, \cdots, 8]$cm in blue, magenta, green, orange, and red lines respectively, (c) the corresponding contours of the approximated torque profile, (d) the rotational spring constant profile.

The resulting rotational spring constant profile $K({\theta_2}^{sta})$ is shown in figure 5(d).

B. Dynamic Movement

As stated earlier, the main objective of our experiments is to explore the influence of internal impedance on dynamic behaviour of perception. Therefore, the dynamic torque, ${\tau_f}^{dyn}$, and angular displacement, ${\theta_2}^{dyn}$ were recorded at different pre-tension states x, during dynamic movement. The dynamic movement trial is carried out by releasing the upper link from a certain angle, i.e. $\theta_2 = 75°$. Data were recorded until the system is settled down to its steady state where $\theta_2 = 0$. An example of such movement is illustrated in figure 6. The measured torque versus rotational displacement trajectory is mapped using a third order best fit polynomial function as shown in figure 7 (a) for each joint stiffness configuration, $x = 4, \cdots, 8$ cm.

C. Perception Information Gain with Transfer Entropy

If we consider τ_f as a random variable, its entropy for a given θ_2 depends on the pre-tension state x. Therefore, the transfer entropy defined in equation 11 - additional information gained about the relationship between τ_f and θ_2 by changing the pre-tension state x - is a good indicator to search for an optimum x [22].

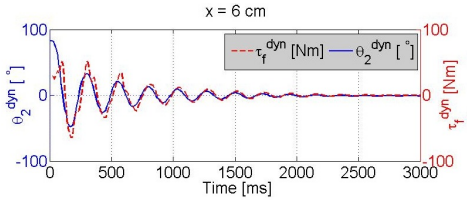

Fig. 6. ${\tau_f}^{dyn}$ and ${\theta_2}^{dyn}$ profiles during the dynamic movement for pre-tension state $x = 6$ cm

$$G = P(\tau_f|x, \theta_2) \log \frac{P(\tau_f|x, \theta_2)}{P(\tau_f|x_{ini}, \theta_2)}, \tag{11}$$

where $G \geq 0$ is the non-negative information gain, $P(\tau_f|x, \theta_2)$ is the probability distribution of dynamic torque over the pre-tension state x and angular displacement θ_2 constructed using 10-trials of static torque data, and x_{ini} is an initial value of x. This implies that if information gain $G = 0$, the joint stiffness has no influence on the causal relationship between ${\tau_f}^{dyn}$ and ${\theta_2}^{dyn}$.

In order to find an optimum pre-tension state x, we use algorithm 1.

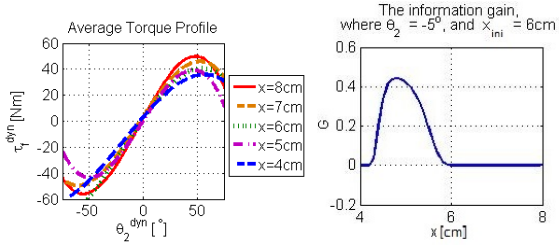

Fig. 7. (a) the best fit third order polynomial functions for the measured dynamic torque profiles, (b) the information gain evaluation with the pre-tension state $x = 4 \cdots 8$ cm; the randomly selected initiaal pre-tension state $x_{ini} = 6$ cm; and the angular displacement of endeffector, $\theta_2 = -5°$.

D. Results: Optimization of Joint Stiffness for Perception

In this paper we compare Newton-Raphson optimization method (requires gradient information) and the Hooke-Jeeves Pattern search method (does not require gradient information) to search for the best x that maximizes transfer entropy G to arrive at a best estimate for θ_2 given the torque measured at the base τ_f.

1) Newton-Raphson Optimization: Newton-Raphson optimization method is a technique to find an extrema in a solution space of a funtion based on a local gradient [23].

Figure 8 depicts this approach in finding the optimum gain when $\theta_2 = -5°$, and $x_{ini} = 6$ cm as an example. The search algorithm for the optimum parameter jump around across iteration and the solution for the 'x_{best}' converges to the local minima of the gain profile resulting in $x_{best} = 6$.

2) Hooke-Jeeves Pattern Search: Hook-Jeeves Pattern Search is a directional search algorithm to obtain the point in the solution space with best fitness. The algorithm was developed by Hooke and Jeeves in 1961 and can be found in *Appendix B* of their paper [24].

Algorithm 1 Algorithm to find an optimum pre-tension state.

Step 1: Choose a set of torque data measured during a dynamic movement of the upper link for a randomly chosen initial pre-tension state x_{ini}.

Step 2: Randomly sample the angular displacement ${\theta_2}^{dyn}$ of the upper link using the relationship corresponding to the x_{ini}, established in figure 7 (a).

Step 3: Construct entropy profile based on ${\tau_f}^{dyn}$ retrieved from random parameters in *Step 1* and *Step 2*, together with the non-linear static memory primitives established in figure 5 (b), and (c).

Step 4: From transfer entropy profile shown in figure 7 (b), search for the best x that would maximize the transfer entropy G profile across x using search algorithms described in section III-D (figure 8 and 9).

Step 5: Use the optimum pre-tension state x_{best} to compute the best approximation ${\theta_2}^{pred}$ of a 'real' ${\theta_2}^{dyn}$ given only the torque reading, ${\tau_f}^{dyn}$ using the static memory primitives corresponding to the x_{best}, established in figure 5 (b).

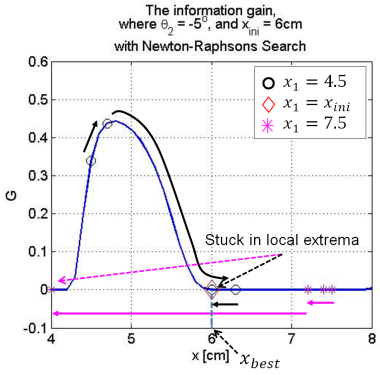

Fig. 8. Implementation of Newton-Raphsons optimization method on a tansfer entropy profile computed at $\theta_2 = -5°$, and $x_{ini} = 6$ cm. The algorithm starts from three different initial points, namely: $x_{start} = 4.5$ cm (black circle), x_{ini} (red trapezoid), and 7.5 cm (magenta star) respectively. The search algorithm finishes the iteration in the local minima for all three starting points. Therefore, utilizing this approach yields $x_{best} \approx 6$.

Hooke-Jeeves Pattern Search is suitable for only unimodal search spaces. Handling a multimodal function with this method may cause the algorithm to get stuck in local maxima. This problem can be minimized by introducing the same dual search approach. An example of this Hooke-Jeeves Pattern Search is shown in figure 9 with the parameter of: $\theta_2 = -5°$, and $x_{ini} = 6$ cm.

The algorithm converges to its maxima of the transfer entropy profile from two starting points, namely: $x_1 = 4.5$ (black circle), and $x_1 = x_{ini}$ (red trapezoid); whereas the algorithm gets stuck in the local minima for the starting point, $x_1 = 7.5$. From this, we obtain the optimum stiffness configuration parameter: $x_{best} \approx 4.8$.

IV. Conclusion

This paper has discussed how a robot with controllable internal impedance can maximize information gain in proprioception by searching for an optimal stiffness under a

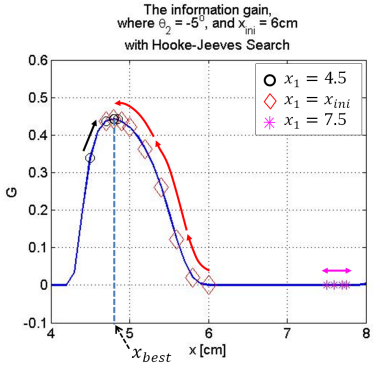

Fig. 9. Implementation of Hooke-Jeeves pattern search method on a tansfer entropy profile computed at $\theta_2 = -5°$, and $x_{ini} = 6$ cm. The algorithm starts from three different initial points, namely: $x_{start} = 4.5$ cm (black circle), x_{ini} (red trapezoid), and 7.5 cm (magenta star) respectively. While, the algorithm with starting point, $x_{start} = 7.5$, gets stuck in the local minima; the rest algorithms converges to the optimum point, $x_{best} \approx 4.8$, of which G is at the maximum.

nonlinear relationship between the entropy of sensor information and the impedance of the physical embodiment. In order to investigate this, we used a laboratory made two link planar manipulator with a McKibben type pivot joint (elbow) with controllable stiffness. Then, we posed the problem of using only torque data measured at the fixed base manipulator, to estimate the deflection at the McKibben type elbow caused by an external force at the free end. There was a unimodal nonlinear relationship between the transfer entropy of proprioception under varying stiffness - determined by the pre-tension state x - of the McKibben type pivot joint. We call it a nonlinear internal memory primitive that the robot can use to enhance proprioception.

In this paper, we provide analytical results and experimental evidence as to how we can exploit such nonlinear memory primitives of embodiment and kinematic variables to enhance the accuracy of the estimation of the internal states of the system during the dynamic behaviours through modulating the internal impedance. Transfer entropy of embodied perception of the internal state - deflection angle of the McKibben type pivot joint in this case - is used as an indicator in searching for an optimal level of pre-tension state for accurate perception. We have compared alternative approaches to enable real-time search of the optimal internal impedance level, namely: Newton-Raphsons Optimization; and Hooke-Jeeves pattern search approach.

The performance of each algorithm is evaluated by the average error in approximation of the θ_2 state. Hooke-Jeeves pattern search method outperforms the Newton-Raphsons optimization approach in term of the average error of approximation of θ_2 as shown in figure 10 (a). Furthermore, though Hooke-Jeeves optimization requires on average more iterations to converge, its corresponding error deviation (shown in error bar) is overall smaller than that of Newton-Raphson Optimization as shown in figure 10 (b).

Based on our results, we speculate that biological counterparts may also be using nonlinear memory primitives similar

to the one demonstrated in this study to tune embodied proprioception. Therefore, it would be interesting to study whether embodiment of muscle spindles (position and speed sensing) and tendons (force/torque sensing) benefits from some real-time internal impedance regulating strategy, and the shapes of the corresponding memory primitives.

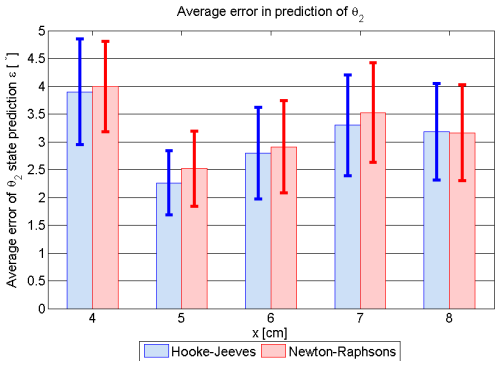

(a)

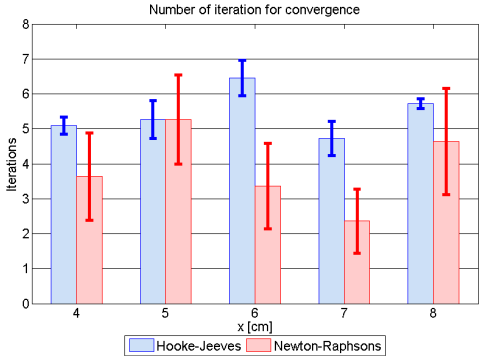

(b)

Fig. 10. (a) The average error of angular displacement, ε, is taken from the average error of prediction of state, ${\theta_2}^{pred}$, with respect to the dynamic angular displacement ${\theta_2}^{dyn}$, ranging from $-10°$ to $10°$, across x_{ini}. The average error along with corresponding error bars produced using Hooke-Jeeves and Newton-Raphsons approach are shown in blue and pink bars respectively, (b) the average number of iterations required until the alternative algorithms - Hooke-Jeeves pattern search (blue bars) and Newton-Raphson optimization (pink bars) - converge with the error bars.

REFERENCES

[1] Å. B. Vallbo, R. Johansson *et al.*, "Properties of cutaneous mechanoreceptors in the human hand related to touch sensation," *Hum Neurobiol*, vol. 3, no. 1, pp. 3–14, 1984.

[2] R. S. Johansson and Å. B. Vallbo, "Tactile sensory coding in the glabrous skin of the human hand," *Trends in Neurosciences*, vol. 6, pp. 27–32, 1983.

[3] M. Lungarella and O. Sporns, "Mapping information flow in sensorimotor networks," *PLoS Comput Biol*, vol. 2, no. 10, p. e144, 10 2006.

[4] M. H. Dickinson, C. T. Farley, R. J. Full, M. A. R. Koehl, R. Kram, and S. Lehman, "How Animals Move: An Integrative View," *Science*, vol. 288, no. 5463, pp. 100–106, Apr. 2000. [Online]. Available: http://dx.doi.org/10.1126/science.288.5463.100

[5] R. Pfeifer, E. Al, R. Pfeifer, M. Lungarella, and F. Iida, "Self-organization, embodiment, and biologically inspired robotics," *Science*, vol. 318, 2007.

[6] A. Jiang, G. Xynogalas, P. Dasgupta, K. Althoefer, and T. Nanayakkara, "Design of a variable stiffness flexible manipulator with composite granular jamming and membrane coupling," in *Intelligent Robots and Systems (IROS), 2012 IEEE/RSJ International Conference on*, Oct 2012, pp. 2922–2927.

[7] A. Jiang, A. Ataollahi, P. Dasgupta, K. Althoefer, and T. Nanayakkara, "A variable stiffness joint by granular jamming," in *ASME 2012 International Design Engineering Technical Conferences and Computers and Information in Engineering Conference*, August 2012, pp. 267–275.

[8] N. Hogan, "Impedance control: An approach to manipulation: Part iii-applications," *Journal of dynamic systems, measurement, and control*, vol. 107, no. 2, pp. 17–24, 1985.

[9] S. Tafazoli, S. E. Salcudean, K. Hashtrudi-Zaad, and P. D. Lawrence, "Impedance control of a teleoperated excavator," *Control Systems Technology, IEEE Transactions on*, vol. 10, no. 3, pp. 355–367, 2002.

[10] K. Mouri, K. Terashima, P. Minyong, H. Kitagawa, and T. Miyoshi, "Identification and hybrid impedance control of human skin muscle by multi-fingered robot hand," in *Intelligent Robots and Systems, 2007. IROS 2007. IEEE/RSJ International Conference on*. IEEE, 2007, pp. 2895–2900.

[11] A. De Luca, A. Albu-Schaffer, S. Haddadin, and G. Hirzinger, "Collision detection and safe reaction with the dlr-iii lightweight manipulator arm," in *Intelligent Robots and Systems, 2006 IEEE/RSJ International Conference on*. IEEE, 2006, pp. 1623–1630.

[12] Y. Yang, L. Wang, J. Tong, and L. Zhang, "Arm rehabilitation robot impedance control and experimentation," in *Robotics and Biomimetics, 2006. ROBIO'06. IEEE International Conference on*. IEEE, 2006, pp. 914–918.

[13] J. W. Sensinger and R. F. Weir, "User-modulated impedance control of a prosthetic elbow in unconstrained, perturbed motion," *Biomedical Engineering, IEEE Transactions on*, vol. 55, no. 3, pp. 1043–1055, 2008.

[14] G. Aguirre-Ollinger, J. E. Colgate, M. A. Peshkin, and A. Goswami, "Active-impedance control of a lower-limb assistive exoskeleton," in *Rehabilitation Robotics, 2007. ICORR 2007. IEEE 10th International Conference on*. IEEE, 2007, pp. 188–195.

[15] J. Aloimonos, I. Weiss, and A. Bandyopadhyay, "Active vision," *International Journal of Computer Vision*, vol. 1, no. 4, pp. 333–356, 1988. [Online]. Available: http://dx.doi.org/10.1007/BF00133571

[16] A. Andreopoulos and J. Tsotsos, "A computational learning theory of active object recognition under uncertainty," *International Journal of Computer Vision*, vol. 101, no. 1, pp. 95–142, 2013. [Online]. Available: http://dx.doi.org/10.1007/s11263-012-0551-6

[17] T. McGeer, "Passive Dynamic Walking," *The International Journal of Robotics Research*, vol. 9, no. 2, pp. 62–82, 1990.

[18] D. N. Beal, F. S. Hover, M. S. Triantafyllou, J. C. Liao, and G. V. Lauder, "Passive propulsion in vortex wakes," *Journal of Fluid Mechanics*, vol. 549, pp. 385–402, Feb. 2006. [Online]. Available: http://www.journals.cambridge.org/abstract_S0022112005007925

[19] J. Liu and H. Hu, "Biological Inspiration: From Carangiform Fish to Multi-Joint Robotic Fish," *Journal of Bionic Engineering*, vol. 7, no. 1, pp. 35–48, Mar. 2010. [Online]. Available: http://linkinghub.elsevier.com/retrieve/pii/S1672652909601840

[20] M. Ziegler, M. Hoffmann, J. P. Carbajal, and R. Pfeifer, "Varying body stiffness for aquatic locomotion," in *2011 IEEE International Conference on Robotics and Automation*. Ieee, May 2011, pp. 2705–2712. [Online]. Available: http://ieeexplore.ieee.org/lpdocs/epic03/wrapper.htm?arnumber=5979798

[21] M. Hoffmann and R. Pfeifer, "The implications of embodiment for behavior and cognition: animal and robotic case studies," *CoRR*, vol. abs/1202.0440, 2012.

[22] R. Van Ham, M. Van Damme, B. Verrelst, B. Vanderbourght, and D. Lefeber, "Maccepa, a mechanically adjustable compliance and controllable equilibrium state actuator: a 3 dof joint with two independent compliances." *Prikladnaya Mekhanika*, vol. 43, no. 4, pp. 130–142, 2007.

[23] T. Schreiber, "Measuring information transfer," *Phys. Rev. Lett.*, vol. 85, pp. 461–464, Jul 2000. [Online]. Available: http://link.aps.org/doi/10.1103/PhysRevLett.85.461

[24] T. Ypma, "Historical development of the newtonraphson method," *SIAM Review*, vol. 37, no. 4, pp. 531–551, 1995. [Online]. Available: http://epubs.siam.org/doi/abs/10.1137/1037125

[25] R. Hooke and T. A. Jeeves, ""direct search" solution of numerical and statistical problems," *J. ACM*, vol. 8, no. 2, pp. 212–229, Apr. 1961. [Online]. Available: http://doi.acm.org/10.1145/321062.321069